Design and optimization of the magnetic circuit of a mobile nuclear magnetic resonance device for magnetic resonance imaging

Hartmut Popella and Gerhard Henneberger
RWTH Aachen, Department of Electrical Machines, Aachen, Germany

Keywords *Magnetic field, MRI, Design optimization, Electromagnetics*

Abstract *The resolution of magnetic resonance imaging, commonly known as MRI, depends on the homogeneity and field strength of the used primary magnetic field $\vec{B}_0$ over the volume of interest. In clinical tomographs homogeneous fields are produced by solenoid coil windings or long round permanent magnets. These solutions are unsuitable for mobile usage because of weight and costs. This paper introduces an optimized magnetic circuit for a mobile universal surface explorer (MOUSE) which meets the requirements of sufficient homogeneity and low weight.*

1. Introduction

The application of nuclear magnetic resonance (NMR) is based on the influence of an externally applied magnetic field $\vec{B}_0$ on the nuclei' orientation. In the presence of an external field the magnetic moment $\vec{\mu}$ will be aligned parallel or anti-parallel towards the $\vec{B}_0$-field and a resulting magnetization $\vec{M}$ will occur. This magnetization processes around the axis of the applied field with the Larmor frequency $f_L = \frac{\gamma}{2\pi} B_0$ (γ: "gyromagnetic" ratio). The aligned magnetization vector can be excited by a high frequency pulse at the Larmor frequency. Only nuclei with $f_L = \frac{\gamma}{2\pi} B_0$ will be affected.

Figure 1 shows the principle design of the MOUSE. The sample (e.g. human tissue, synthetic material) should be placed onto the measuring instrument. This design restriction causes an inhomogeneous field-strength distribution. The B_0-field decreases with increasing y-coordinate; the decrease of the field along the y-axis follows the equation $B = B_0(y = 0) \cdot a^{-ky}$ with $a > 1, k > 0$. For magnetic resonance imaging a linear field gradient is required because only certain spins in selected slices Δy of the sample should be in resonance. In the case of the considered NMR-MOUSE the penetration depth is the y-axis. In the selected slice Δy only nuclei which meet the frequency requirement $\Delta f = \frac{\gamma}{2\pi} \Delta B_0$ are excited by a high frequency pulse with the bandwith Δf. Only these nuclei contribute to the test signal. Because of the wanted linear gradient there is a linear relationship between the bandwith Δf and the slice thickness Δy.

A small linear gradient $\frac{\Delta B_0}{\Delta y}$ of the main field B_0 effects a small bandwith Δf (corresponding to $\Delta f \sim \Delta B_0$) field which is easier to produce. A high

COMPEL : The International Journal for Computation and Mathematics in Electrical and Electronic Engineering, Vol. 20 No. 1, 2001, pp. 269-278.

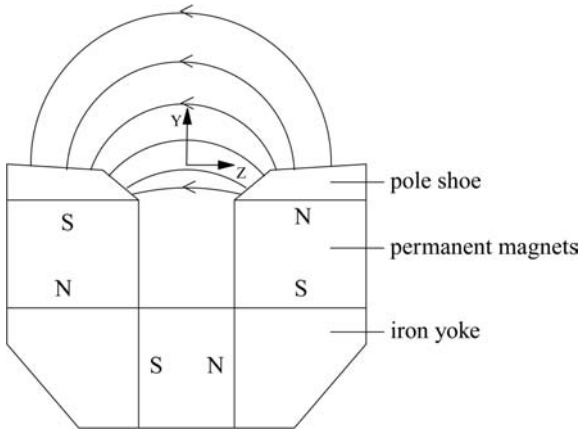

Figure 1.
Principle of the NMR-MOUSE

magnitude of B_0 provides a better signal-to-noise-ratio because of the proportionality $S \sim B_0^{\lambda}$ with $1 < \lambda < 2$ (Hausser and Kalbitzer, 1989). Besides, a large gradient deteriorates depth of penetration. Figure 2 demonstrates the effect of non-linear B_0-field decrease on the depth of penetration. Either the required bandwith Δf becomes larger for the same depth of penetration, or the selected slice-thickness becomes smaller for the same bandwith ($\Delta y_1 < \Delta y_2$). Therefore a linear field distribution with a small gradient is necessary at least over a short distance from the MOUSE surface. A small gradient, a high main field B_0 and low weight of the magnetic circuit are the demands on the NMR-MOUSE.

For a detailed introduction to nuclear magnetic resonance (relaxation processes) and image reconstruction (two-dimensional Fourier imaging) it is referred to literature dealing with NMR and MRI (Jin, 1999; Vlaardingerbroeck and de Boer, 1996; Kimmich, 1997). A description of hollow cylindrical tomographs for clinical applications can be found in Zijlstra (1985).

2. 2D calculations

The following examinations are limited to 2D calculations and optimizations.

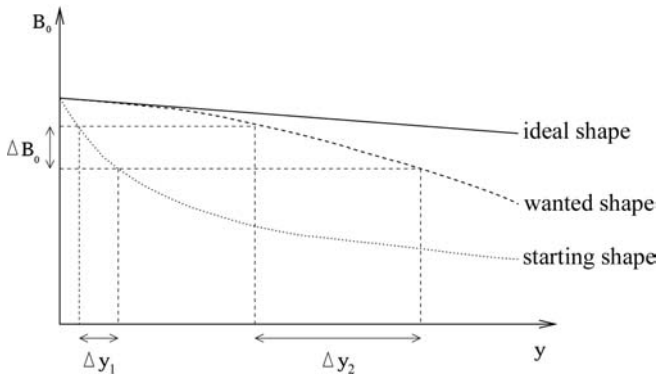

Figure 2.
Starting and wanted field-strength distribution in comparison to ideal homogeneity; $\Delta B_0 = \frac{\Delta\omega}{\gamma} = \frac{\omega_1 - \omega_2}{\gamma}$

2.1 Field calculations

The B_0-field is a pure static magnetic field and therefore the magnetic vector potential formulation $\vec{B} = \nabla \times \vec{A}$ is used for solving the FEM-problem. This formulation is implemented in the solver of the commercial FEM-program ANSYS. ANSYS is used for the following presented results.

2.2 Pole shoe shape influence on B_0-field

An empiric examination of different pole shoe shapes is hardly possible without a suitable aid because the pole shoe coordinates must be changed for each new pole shoe shape. A program automates this series (Figure 3). The following pole shoe shapes in Figures 4 and 5 have a height of 10mm, the airgap is 45mm, the dimensions of the lower horizontal magnet are 45mm × 80mm, those of the vertical magnet are 80mm × 80mm. These pole shoes only represent a selection of investigated pole shoe shapes. Figure 6 shows that the pole shoe shape does not affect the gradient of B_0 in y-direction. The most suitable pole shoe geometries regarding a high flux density B_0 are the models one and three (from the left side) in Figures 4 and 5.

3. Deflection magnets

The results above demonstrate that a simple C-core with pole shoes upon the magnets does not affect the gradient. For this reason a deflection magnet (Figure 7) which is magnetized in x-direction is attached in the airgap. By using deflection magnets it is possible to achieve an almost constant field distribution at least for the first 10mm in y-direction. The position of the deflection magnet (Figure 8) in the airgap is important for the B_0-shape as it is shown in Figure 9. This position has an effect on the gradient of B_0 as well as on the induction value and can avoid a local maximum of B_0-field distribution which is in the way of image reconstruction. An optimization tool is used in order to find suitable dimensions of the used magnets.

4. Design optimization

The optimal gradient shape combined with a high field strength is achieved by an optimization loop. The FEM-program ANSYS offers different optimization tools (ans,). There are three types of optimization variables:

(1) The independent variables are called design variables.

$$\vec{x} = (x_1\ x_2 \cdots x_n) \tag{1}$$

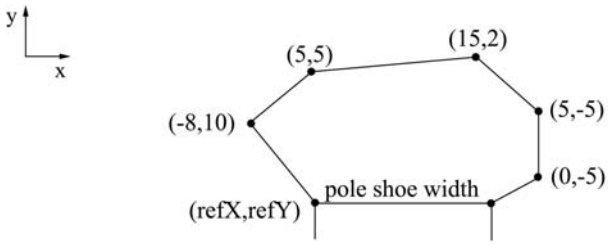

Figure 3.
Defining pole shoe shapes by using relative coordinates

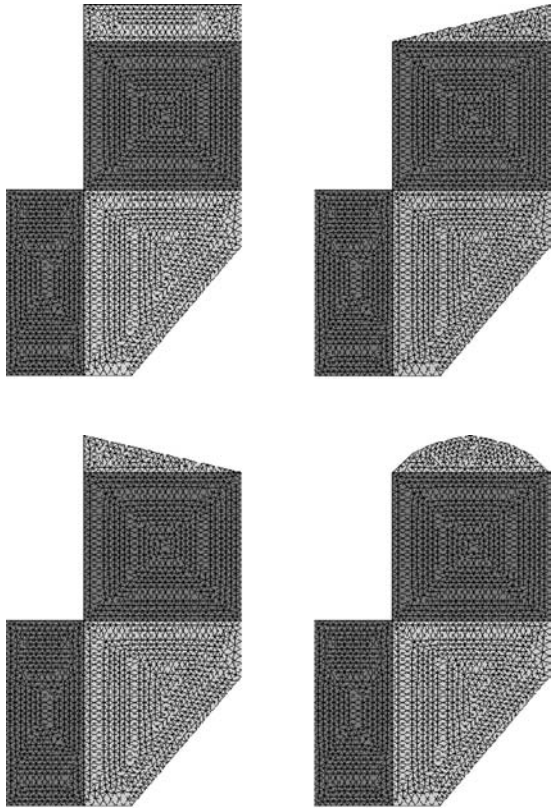

Figure 4.
Pole shoe 1 and 2

Figure 5.
Pole shoe 3 and 4

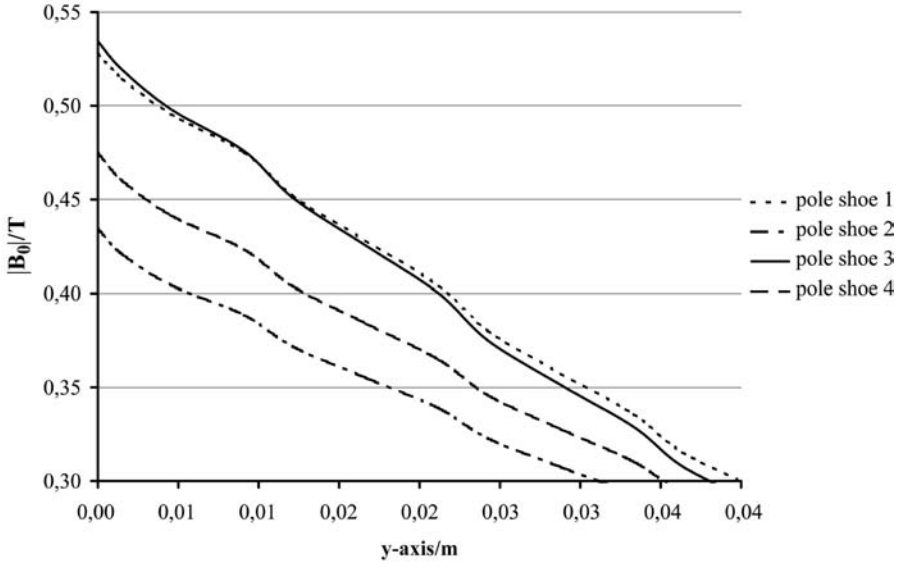

Figure 6.
Comparison of different pole shoe shapes

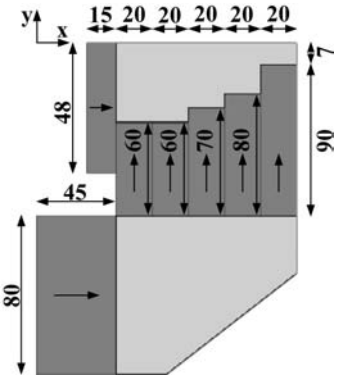

Figure 7.
Proportions for arrangements with deflection magnets

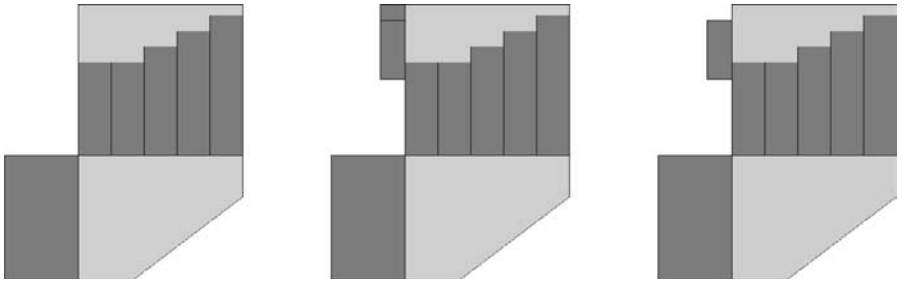

Figure 8.
Arrangements without and with (1,2) deflection magnets. The position of the deflection magnets can be varied

They determine the geometry of the NMR-MOUSE such as magnets' height and width and position of the deflection magnet. Design variables can be changed by the optimization algorithm in order to fulfil certain requirements expressed by state variables. Design variables are restricted by lower and upper limits:

$$\underline{x}_i \leq x_i \leq \overline{x}_i (i = 1, 2, \ldots, n) \tag{2}$$

These limits depend on the allowed or wished dimensions of the NMR-MOUSE. For example, one aim of the optimized NMR-MOUSE is a certain weight that must be kept. For this reason there are certain design restrictions regarding the external dimensions of the MOUSE.

Definitely the following five parameters have been chosen as design variables for 3D calculations:

- Width of airgap.
- Depth of airgap.
- Width and height of the main vertical magnets on the left and right side of the NMR-MOUSE.
- Depth of the inner vertical magnets (modified deflection magnets, Figure 13) next to the main vertical magnets.

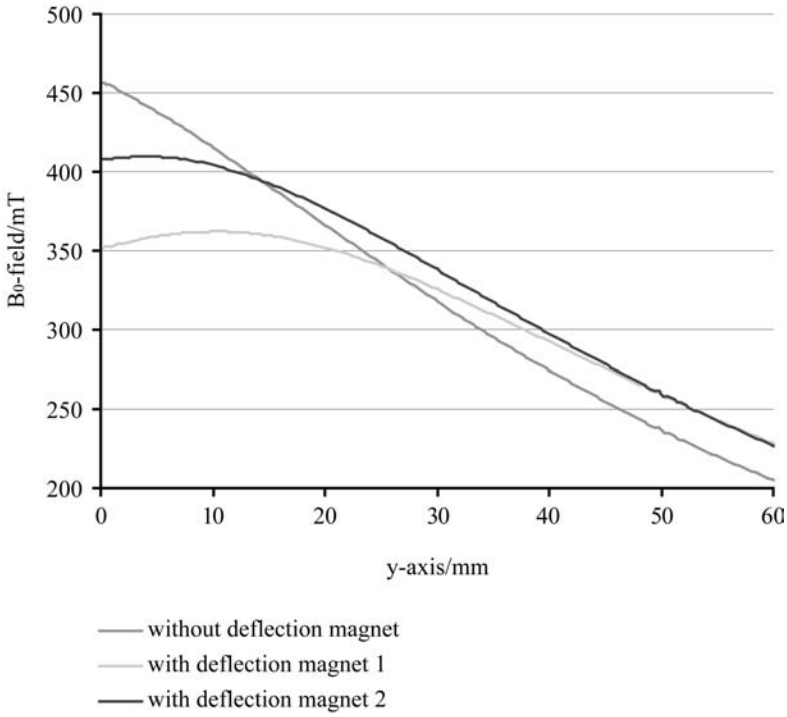

Figure 9.
Comparison of arrangements with deflection magnets

In ANSYS up to 60 design variables can be defined, but an increasing number of design variables reduces the chance of finding an optimal arrangement for the NMR-MOUSE because of too many possible variations within the lower and upper limits ($\underline{x}_i \leq x_i \leq \overline{x}_i$) of all defined design variables.

(1) The optimization algorithm tries to minimize the objective function

$$f = f(\vec{x}) \tag{3}$$

so that state variables are kept. The objective function is a weighted function of the required gradients. The following term defines the objective function as a function of desired field gradients, absolutely wanted flux density values B_0 along the penetration depth (y-axis, Figure 1) and weight of the NMR-MOUSE which depends on the design variables $\vec{x}$:

$$f(\vec{x}) = \frac{dB_0(y)}{dy}|_{x=0} + \frac{B_0(y = 0\text{mm})}{0.25\text{T}}|_{x=0} + \frac{B_0(y = 20\text{mm})}{0.225\text{T}}|_{x=0} + weight_{MOUSE}(\vec{x}) \tag{4}$$

(3) The state variables are defined by the necessary field strength $B_0(y_i)$ in a certain depth of penetration. The optimized magnetic circuit should supply required flux density within defined limits at $y = 0$mm,

$y = 20\text{mm}$ and $y = 40\text{mm}$.

$$\underline{w}_i \leq w_i(\vec{x}) \leq \overline{w}_i \tag{5}$$

NdFeB has been chosen as magnetic material for all optimization loops. For the final optimized geometry the magnetic characteristics of the used NdFeB material are:

- remanence flux density = 1.33T
- coercive field strength = $796\,\frac{\text{kA}}{\text{m}}$

5. Verification of FEM calculations' accuracy

A way of influencing the gradient of the NMR-MOUSE has been introduced for 2D calculations. In contrast to electrical machines there is a great airgap and no surrounding iron yoke. The accuracy of the FEM-calculations essentially depends on the amount of integrated air volume. An increasing number of air elements with $\mu_R = 1$ decreases the induction value B_0 along the y-axis. For this reason a far-field boundary condition is used. A verification of the FEM-calculated solution is the comparison of solutions with far-field boundary conditions to solutions with Dirichlet boundary conditions on the boundary of the FEM domain. The solution with Dirichlet boundary conditions should converge to that with far-field boundary conditions if the integrated air volume expands. Table I verifies this assumption for penetration depths at $y = 0\text{mm}$ (on the MOUSE surface), $y = 20\text{mm}$ and $y = 40\text{mm}$.

First order triangle elements (plane13 in ANSYS) have been chosen for two dimensional calculations, tetrahedral elements (solid97 in ANSYS) for three dimensional calculations. The unbounded problem has been modelled by infin110 (2D) and infin111 (3D) elements with four (2D) and eight (3D) nodes respectively. Figure 10 shows the meshed magnets.

Penetration depth/mm	Far-field boundary conditions B_0/mT 30cm air	Dirichlet boundary conditions B_0/mT 30cm	60cm	90cm	150cm
0	352.16	379.00	359.80	355.76	353.65
20	353.02	376.71	359.56	356.00	354.15
40	294.25	315.55	300.06	296.92	295.27
Number of elements	14.186	15.017	26.967	43.593	90.850
Number of nodes	7.329	7.735	13.912	22.426	46.458
Computation time/ min:sec	1:22.1	1:33.5	2:41.1	4:22.1	9:17.9
Disk space/MB used by ANSYS result files	18	33	57	86	178

Table I. Comparison of 2D solutions with infinite boundary elements to 2D solutions with conventional boundary condition

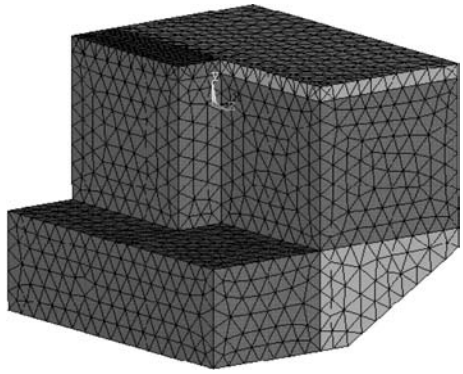

Figure 10.
Meshed FEM-model for the magnets

6. 3D calculations

6.1 Elimination of stray flux

A large problem of 3D calculations is the appearing stray flux in z-direction. Table II shows the influence of model's depth. For these calculations the introduced 2D arrangement with deflection magnets within the airgap was maintained and only extruded in z-direction. One can draw the conclusion that two dimensional optimizations are insufficient for the NMR-MOUSE because of the amount of surrounding air. There are two main parameters which influence the stray flux and the gradients' shape:

- The airgap influences the gradient's shape; a larger airgap provides a linear gradient shape (Figure 11).
- The depth of the NMR-MOUSE decreases the stray flux' effect on B_0-induction along the y-axis (Figure 12).

Therefore the two dimensionally found geometry with deflection magnets and the position of the deflection magnets within the airgap must be slightly modified. Figure 13 shows the principle design of the modified prototype.

The plain iron pole shoe is necessary in order to avoid a local maximum of B_0-induction shape which is a strictly monotonic function, as Figure 14 demonstrates.

6.2 Reduction of weight

The weight of this arrangement can be reduced by using highly remanent NdFeB magnets. Besides the demand for low weight, a high magnitude of B_0-

Penetration depth/mm	2D calculations B_0/mT	3D calculations B_0/mT				
0	352.16	42.75	116.79	198.33	275.05	299.32
20	352.06	91.09	158.12	230.16	290.48	307.93
40	292.52	82.64	138.43	197.7.0	245.59	259.10

Table II.
Comparison of different model depths for the NMR-MOUSE

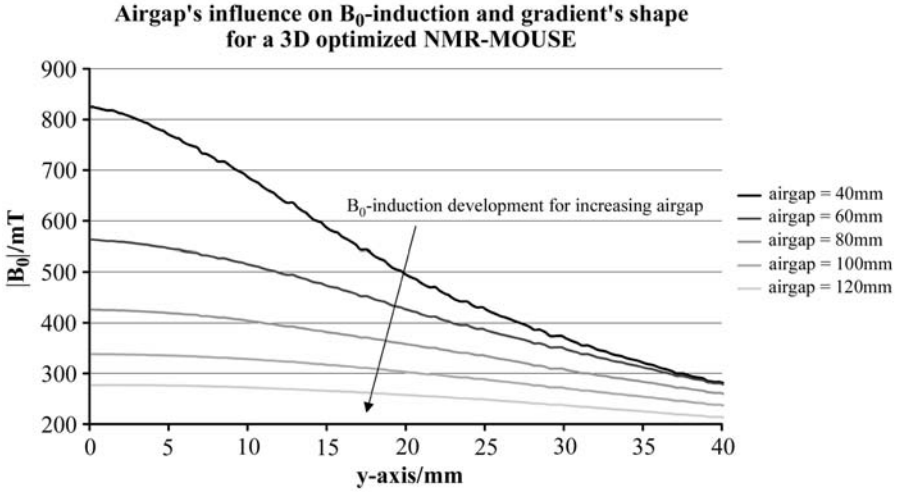

Figure 11.
Influence of the airgap of the NMR-MOUSE

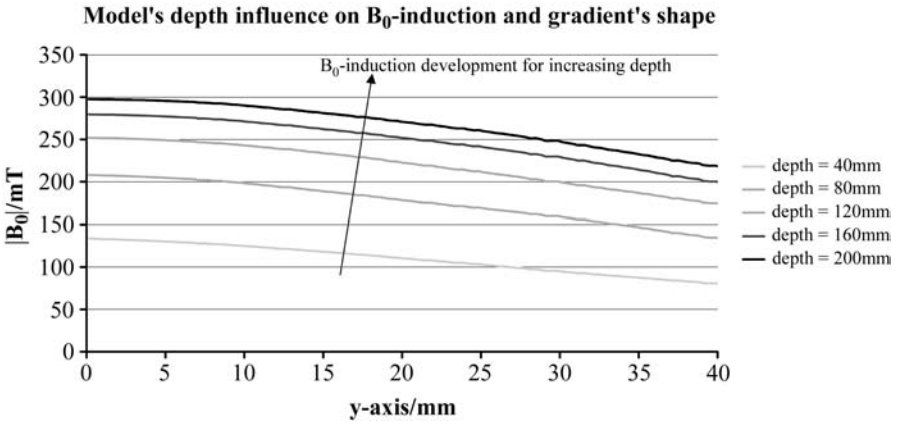

Figure 12.
Influence of the depth of the NMR-MOUSE

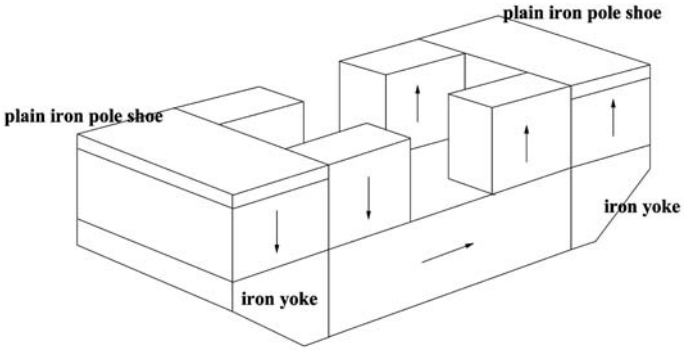

Figure 13.
Prototype of the NMR-MOUSE with modified deflection magnets

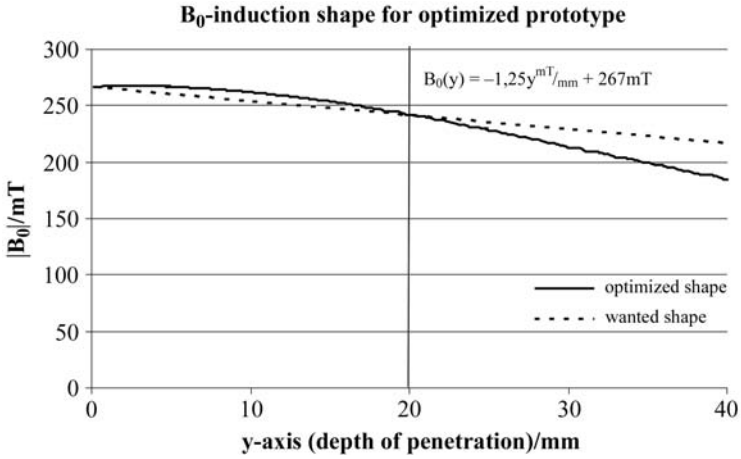

Figure 14.
B_0-induction shape for the optimized prototype

induction and a small gradient are contradictory. One can state that field strengths above $B_0(y = 0) = 250mT$ and $\frac{\Delta B_0}{\Delta y} = 1.25\frac{T}{m}$ can only be realized with use of much magnetic material (>30kg). This weight and costs contradict the mobile application of the MOUSE. A possibility of reducing weight may be a cylindrical magnetic arrangement. The surrounding permanent magnets have a certain magnetization direction. On the one hand, this arrangement reduces the total weight up to 50 percent, on the other hand, it produces a tangential and not a normal field distribution concerning the y-axis.

7. Conclusion

In this paper a way of influencing the gradient and reducing stray flux and weight of the NMR-MOUSE has been introduced. 2D modelling and the use of pole shoes are unsuitable for this kind of application.

References

ANSYS Advanced Analysis Techniques, Design Optimization.

Hausser, K.H. and Kalbitzer, H.R. (1989), *NMR für Mediziner und Biologen*, Springer-Verlag, New York, NY.

Jin, J. (1999), *Electromagnetic Analysis and Design in Magnetic Resonance Imaging*, CRC Press, Boca Raton, FL.

Kimmich, R. (1997), *NMR, Tomography Diffusometry Relaxometry*, Springer-Verlag, New York, NY.

Vlaardingerbroeck, M.T. and den Boer, J.A. (1996), *Magnetic Resonance Imaging: Theory and Practice*, Springer-Verlag, New York, NY.

Zijlstra, H. (1985), "Permanent magnet systems for NMR tomography", *Philips Journal of Research*, Vol. 40, pp. 259-88.